Progress In Electromagnetics Research M, Vol. 96, 9–20, 2020

An Ultra-Thin Non-Resonant Class of Frequency Selective Surface for X Band Applications

Vahida Shaik* **and Shambavi Krishnan**

Abstract—A new miniaturized and ultra-thin non-resonant element-class of convoluted frequency selective surface (FSS) structure with reduced overall thickness is presented and empirically verified. The proposed FSS structure, which could be capable of providing a first order narrow band pass response for X band applications, is made up of three metallic layers separated from one another by two dielectric substrates. The outer layers are made up of convoluted inductive grids, and the inner layer is a non-resonant structure composed of convoluted square slot array. A first-order band pass response FSS with a centre frequency of 10.5 GHz and fast roll-off characteristics is presented. The overall element thickness of the proposed FSS is $\frac{\lambda}{56}$, which is smaller than previously proposed miniaturized structures. The comparison between all patch layers with the proposed structure which is not an all patch layers is explicated in detail with its convoluting effects. The validity of this design procedure is verified with an equivalent circuit model, and a sample is fabricated and measurement done using a WR 90 waveguide setting for experimental verification.

1. INTRODUCTION

Frequency selective surface (FSS) applications have recently dominated not only the fields of microwave and terahertz regime shielding, radar cross-section reduction, THz sensing, detection, and as absorbers, but also in several other applications. These include radio astronomy [1], energy harvesting applications [2], energy-efficient glass [3], microwave lenses [4], beam switching applications [5], ultra-wideband radio frequency identification tags [6], wireless charging pads for portable electronics [7], and pulsed high power microwave applications [8, 9]. Conventional FSS is of limited use because of its narrow bandwidth and unstable characteristics. Recently, miniaturization has become a fundamentally important criterion for all wireless communication applications and is essential for radomes, mobile communications, and portable electronics applications. Researchers use the technique of convoluting (meandering) the FSS structure [10], or of using fractal-based structures [11] for miniaturization. A novel miniaturized element FSS comprising an array of metallic patches with a capacitive surface and a coupled inductive grid acting as a resonant circuit with angle-of-incidence sensitivity for single and dual pole responses was first proposed in [12].

In 2009, Al-Joumayly and Behdad proposed a non-resonant structure, which used sub-wavelength unit cell structures where the overall thickness and unit cell periodicity was much smaller than in conventional systems [13]. All-inductive sub-wavelength inductive grids which are separated by two dielectric substrates with a higher-order band pass response [14] and miniaturized resonant elements with non-resonant and hybrid layers in the middle have been reported with second- and third-order band pass responses [15, 16]. A structure involving two capacitive layers separated by an inductive patch layer has been presented for its second-order band pass response and as a polarization converter which produced a circularly polarized wave when being illuminated by a linearly polarized plane wave [17].

Received 25 June 2020, Accepted 9 August 2020, Scheduled 27 August 2020
* Corresponding author: Vahida Shaik (vahida.sk@gmail.com).
The authors are with the School of Electronics and Communication Engineering, Vellore Institute of Technology, Vellore, India.

To produce additional poles and zeros, a hybrid resonator was placed in between two inductive layers to achieve third-order resonance as reported in [16]. This miniaturized-element frequency selective surface (MEFSS) not only reduced the unit cell size, but also provided stable characteristics for dual-polarization. The first order design MEFSS bandwidth was limited, so all patch layers were designed to achieve higher bandwidth characteristics. As reported in [18], a patch layer structure, in which all four square patch element layers were separated by an inductive non-resonant layer with higher bandwidth, was used for X and Ku bands. To achieve miniaturization, meandering/convoluting of the structure or fractal geometries have been used by several researchers. The convoluted structures provide highly stable characteristics and accurate results, but the most convoluted and interwoven structures fabrication is difficult and requires high precision fabrication processes.

To address these issues, 2.5D [19] and 3D structures [20] have recently been reported for further miniaturization of the unit cell. In a recent study, a double-layer, ultra-miniaturized FSS was proposed for improved miniaturization, which achieved a resonant frequency of 2.16 GHz. One side was made up of a convoluted slot grid and the other side made up of a convoluted slot dipole. It was also realized by cascading four convoluted slot grids with one layer of convoluted slot dipoles for an ultra-miniaturized unit cell size of $0.019\lambda \times 0.019\lambda$ [21].

In the present study, four structures have been analyzed, both with and without simple convolution of the inductive grid layers. The structural design steps are discussed along with their simulated results to compare the effects of convolution. The structure was then fabricated, comprising a convoluted inductive grid array as a resonant layer, sandwiched between the non-resonant convoluted square slot arrays. The design concept involved a convoluted inductive grid layer, which was separated from a non-resonant middle layer comprising a combination of two series inductive grids in parallel with an edge convoluted square slot. However, the proposed structure provided only a band pass response at 10.5 GHz. The overall thickness of the proposed FSS was 0.0177λ, where λ is the free space wavelength corresponding to the resonant frequency of the proposed FSS structure which was very small compared to the conventional FSS proposed earlier. The unit cell size of the proposed band pass FSS was $0.1752\lambda \times 0.1752\lambda$. Several parametric analyses were applied to achieve the desired result. The main comparison among all inductive grid layers or patch layers (Structures 1, 2, and 3) with the proposed structure (not all patch layers) with its convoluting effects was described in different stages. All the simulations are performed with the HFSS (high frequency structure simulator) software using EM (electromagnetic simulation) simulation method. To validate the design, a sample was fabricated and tested using waveguide measurement.

2. UNIT CELL STRUCTURE STAGES

In this design, the width of the inductive top and bottom layers was $w = 0.4$ mm with a unit cell size of $P = 5$ mm in both the x and y directions. The length of all four L-shaped patches was $L = 2.1$ mm, and the width of the L-shaped inductive patches was $d = 0.1$ mm with a middle slot spacing of 0.4 mm. RT Duroid 5870 dielectrics with a dielectric constant of 2.33, a dielectric loss tangent of 0.0012, and a thickness of 0.25 mm were used.

2.1. Structure 1

A basic resonant inductive grid layer on top and bottom with non-resonant four L-shaped patches used in middle layer was designed. Fig. 1 shows the unit cell of the FSS comprising an inductive grid layer on top and bottom layers and four L-shaped patches forming a square patch non-resonant layer in the middle. All four L-shaped patches were placed in such a way as to maintain a spacing of 0.4 mm between them when being covered by the upper and bottom inductive layer widths. When the spacing 'S' changed, the resonant frequency also changed. A larger spacing led to a higher resonant frequency, while a smaller spacing led to a lower resonant frequency.

However, the stability was higher when the spacing was larger, whereas when the spacing was smaller, at approximately 0.1 mm, stability was not maintained for both the transverse electric (TE) and transverse magnetic (TM) polarizations. Here stability refers to the angular stability for oblique angles of incidence for horizontal and vertical polarizations. As the spacing 'S' varied from 0.6 to 0.2 mm

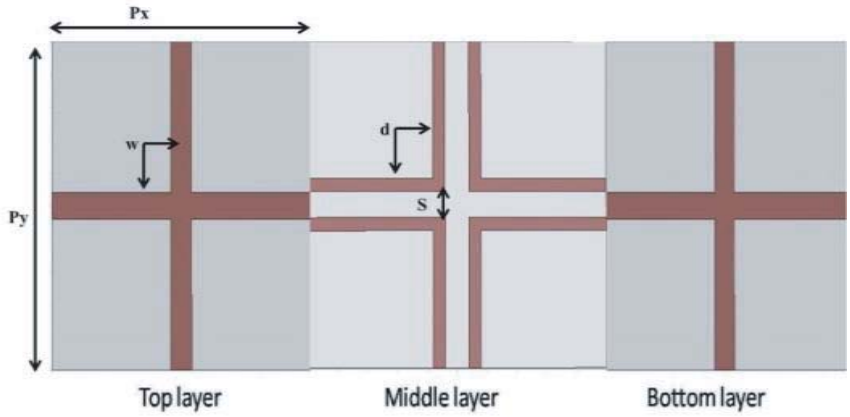

Figure 1. Geometry of the structure 1 unit cell.

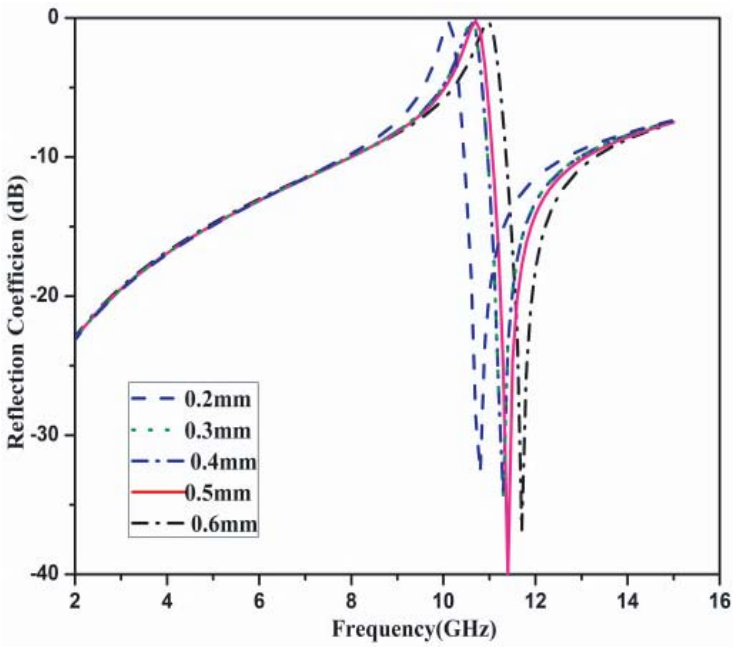

Figure 2. Frequency response of reflection coefficient as a function of spacing.

with a fixed L-shaped patch width of $d = 0.1$ mm, the resonant frequency varied accordingly. When the L-shaped patch width varied, the resonant frequency varied from a higher to a lower frequency. However, the stability was good only when the spacing was 0.3 mm or 0.4 mm. The spacing between the L-shaped patches and the spacing of the top and bottom layers had a profound effect on stability and the resonant frequency, as shown in Fig. 2. The passband resonant frequency that was achieved was approximately 11 GHz at spacing of 0.4 mm, which was the same as the top and bottom layer patch widths.

2.2. Structure 2

Convolution of the structure allows for miniaturization. The top and bottom metal arrays meandered with a gap of $g = 0.1$ mm as shown in Fig. 3. The meandering of the structure of the top and bottom layers allowed a passband resonant frequency of approximately 8.8 GHz to be achieved. The conventional structure without meandering yielded a passband frequency of 11 GHz, whereas meandering

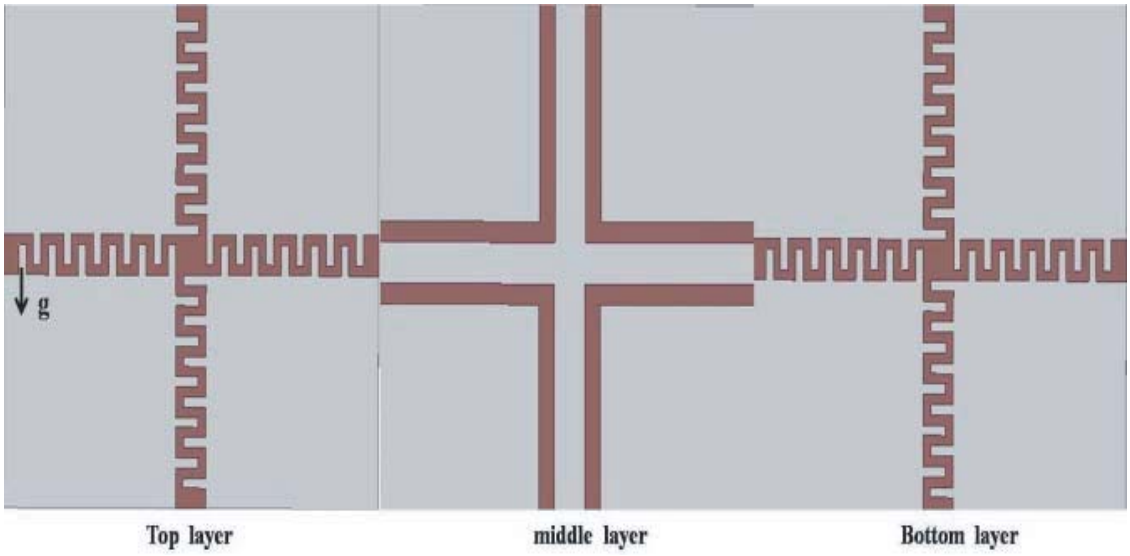

Figure 3. Geometry of the structure 2 unit cell.

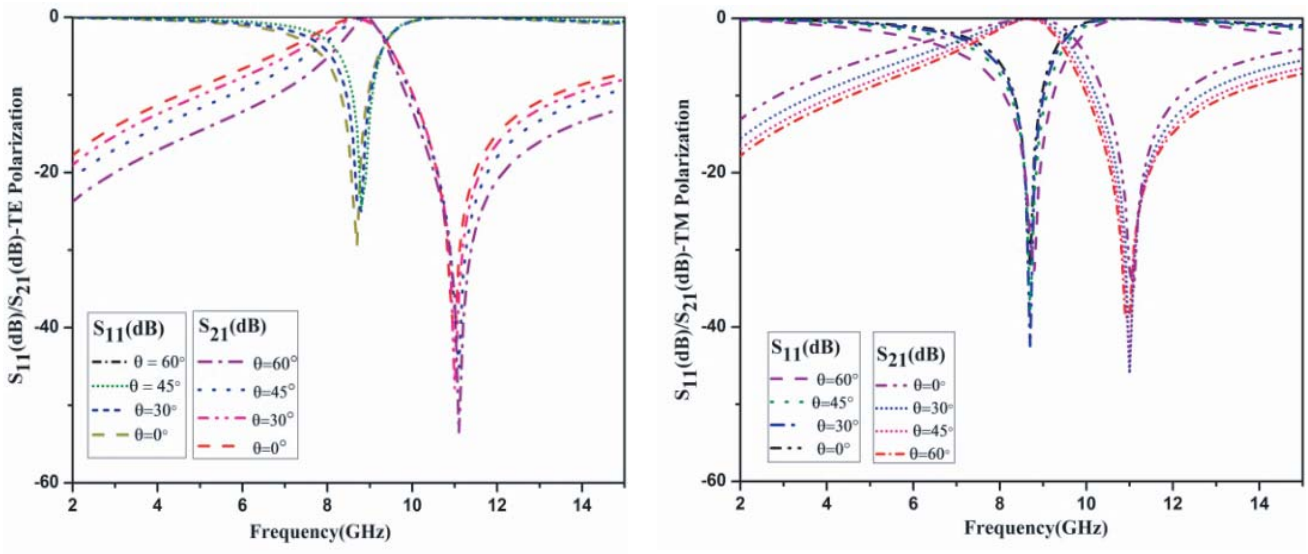

Figure 4. (a) Simulated TE polarization of structure 2 for different angles of incidence. (b) Simulated TM polarization of structure 2 for different angles of incidence.

the structure reduced this to approximately 2.2 GHz. The stopband had a high transmission coefficient (TC) of more than 50 dB insertion loss at 11.1 GHz, along with a bandwidth from 9.9 GHz to 15.8 GHz. Good stability was achieved for this structure for both the passband and stopband frequencies. This FSS structure provided more than 20 dB insertion loss for both the passband and stopband resonant frequencies. Transmission and reflection behaviourd for both the TE and TM polarizations of structure 2 are shown in Figs. 4(a) and 4(b).

2.3. Structure 3

The previously discussed structure reduced the frequency from 11 GHz to 8.8 GHz, so work begun on further miniaturization by convoluting the middle layer, which is a non-resonant layer shown in Fig. 5.

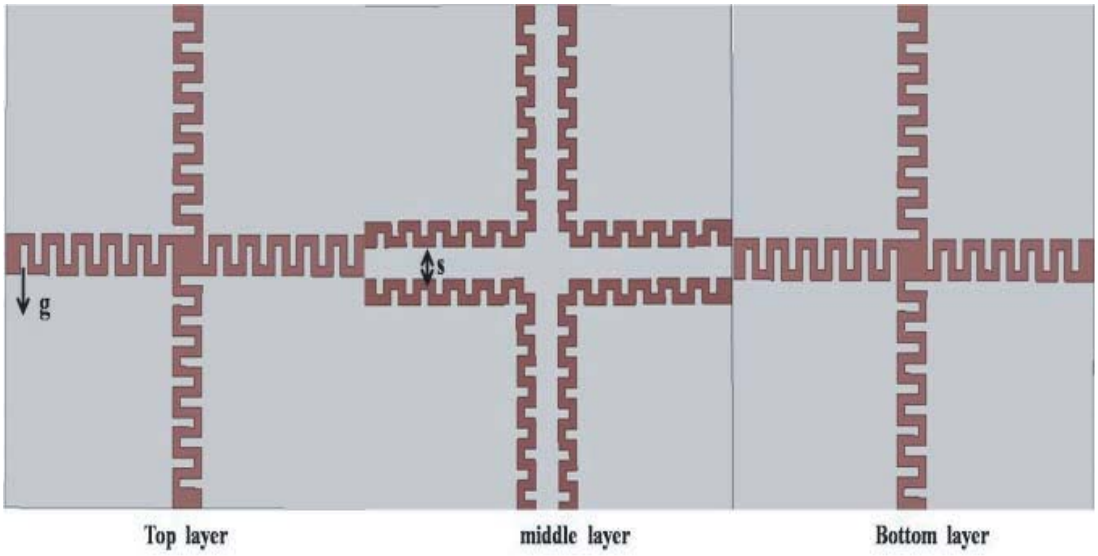

Figure 5. Geometry of the structure 3 unit cell.

The passband frequency shifted to a lower frequency at approximately 7.9 GHz, and the stopband frequency also decreased. Using this structure, the transmission coefficient (TC) and reflection coefficient (RC) values were approximately −40 dB and more, in both the passband and stopband frequencies, with high stability characteristics for both polarizations. For different oblique angles of incidence and for TE polarization, the insertion loss was reduced when the angle of incidence increased, whereas for TM polarization, the insertion loss increased when the angle of incidence increased.

From Fig. 6, it can be seen that the bandwidth varied with varying oblique angles of incidence. However, the centre frequency was 7.9 GHz for both TE and TM polarizations with a minor shift in frequency at an angle of incidence of 45° and above. However, the transmission coefficient and reflection coefficient values that were achieved were good and very high for a stopband frequency. Applications

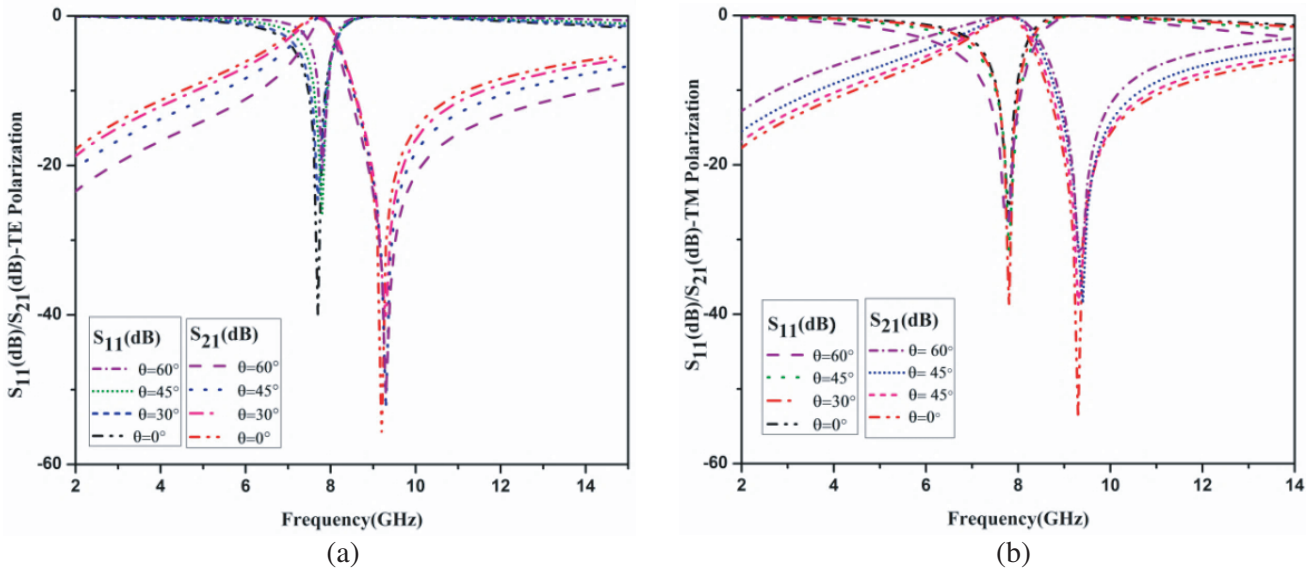

Figure 6. (a) Simulated TE polarization of structure 3 for different angles of incidence. (b) Simulated TM polarization of structure 3 for different angles of incidence.

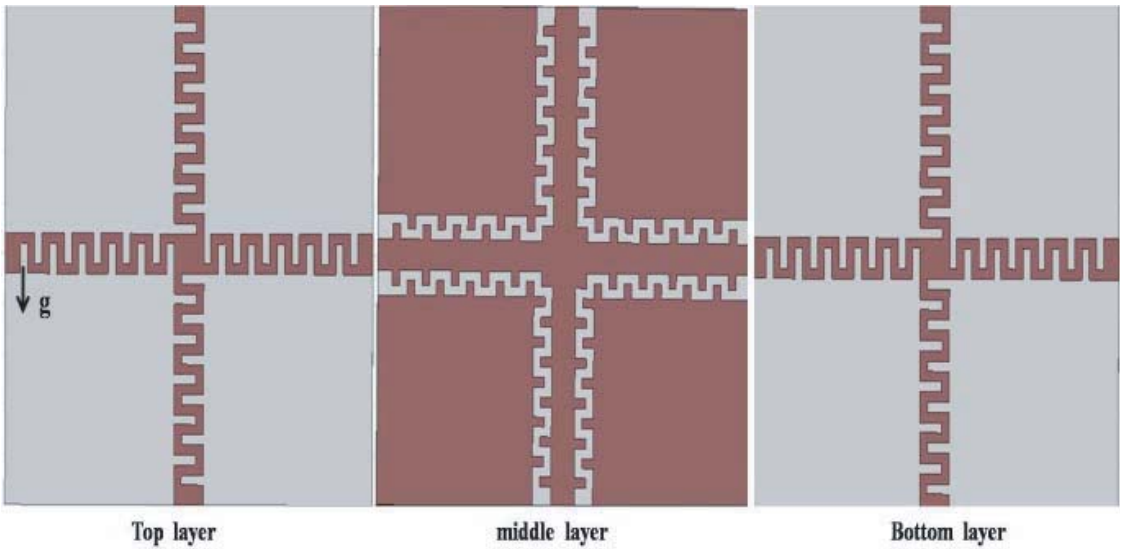

Figure 7. Geometry of the proposed FSS.

that require upper X-band frequency shielding and an 8 GHz passband frequency may find this structure useful. In comparison with structure 2, for polarizations, the TC and RC values for this structure were higher, which indicated that the miniaturization not only reduced the resonant frequency, but also increased the TC and RC values as can be seen in Fig. 6(a) and Fig. 6(b). The passband characteristics at 7.9 GHz demonstrated a narrow bandwidth ranging from 7.1 GHz to 8.2 GHz with a −40 dB RC at 7.9 GHz.

3. PROPOSED FSS AND SIMULATION RESULTS

The above three structures where all three layers are inductive patches, with and without convoluting structures described with its effects of frequency and stability with oblique angles of incidence and polarization. In this proposed structure, the top and bottom layers are same convoluted inductive grid layers, where as in the middle layer instead of inductive grid layer here we introduced a square slot array layer. The major difference that one could observe was that it provides only a band pass filtering response, and there is no other band stop filtering response and grating lobes for higher frequencies.

The proposed FSS contained three metallic arrays separated by a thin dielectric substrate. The top and bottom metallic array is composed of a convoluted inductive grid array, and the middle one composed of a non-resonant miniaturized convoluted square slot array. Fig. 7 and Fig. 8 show the unit cell structures and their isometric projection view. The proposed FSS resonated at a centre frequency of 10.5 GHz. The conventional structure discussed in the structural design step 1 yielded a 13.8 GHz resonant frequency, whereas the proposed FSS with non-resonant convoluted square slot structure and a convoluted inductive grid array of resonant layers achieved a resonant frequency of 10.5 GHz band pass filtering with good angular stability. In the proposed design, there were no stopband characteristics, and only a band pass filtering response could be perceived. Grating lobe generation was not noted, which ensured smooth and fast roll-off characteristics.

The proposed structural design can be seen in the three-dimensional isometric projection of 5×2 elements in Fig. 8.

The fractional bandwidth achieved at a normal angle of incidence was approximately 42%. The simulated transmission loss was above −35 dB for perpendicular polarization and above −50 dB for parallel polarization. The proposed structure was useful for X band applications and was stable at oblique angles of incidence greater than or equal to 40° with only small variation. Only 0.1 GHz variation was observed in TE when the angle of incidence increased, whereas in TM, only at an angle

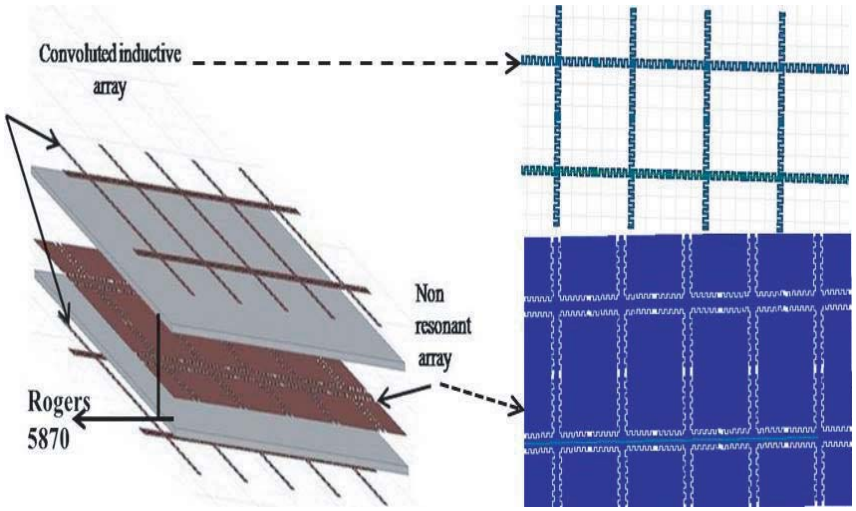

Figure 8. Isometric projection of the proposed FSS.

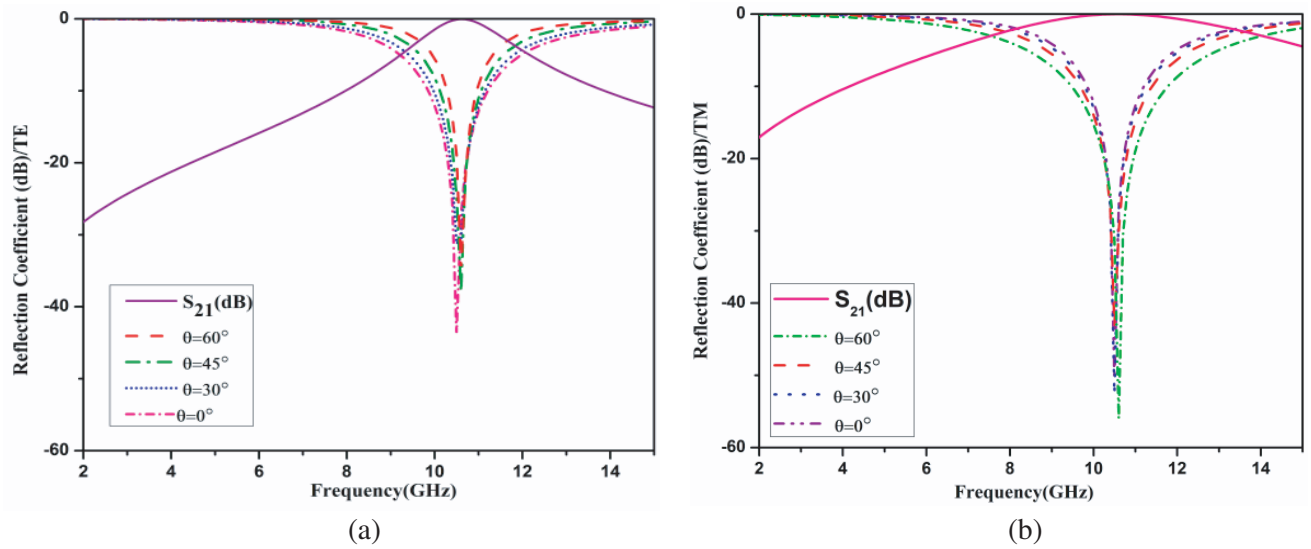

Figure 9. (a) Reflection behaviour of FSS at oblique angles of incidence for TE mode. (b) Reflection behaviour of FSS at oblique angles of incidence for TM mode.

of incidence of 60° the centre frequency shifted to the next highest frequency of 10.6 GHz with high RC values. The reflection behaviour of the proposed structure can be seen in Figs. 9(a) and 9(b) for various oblique angles of incidence and for both polarizations.

The proposed structure's dielectric substrate thickness was significantly less than that of conventional structures when operating at approximately 10.5 GHz. When the dielectric substrate was made thicker, the order of the filter response increased (14, 15, and 16), and it also reduced the fractional bandwidth. The fractional bandwidth was larger in the proposed structure because of the thin dielectric substrate and the non-resonant layer characteristics of the middle layer. Conventional FSS structure bandwidths depend on the inter-element spacing. The larger the spacing is, the narrower the bandwidth is. The smaller the spacing is, the higher the bandwidth is. The proposed structure's middle layer inductive characteristics with its low capacitance had an intense effect on the bandwidth and resonant frequency performance characteristics. The surface current distribution at the centre frequency of 10.5 GHz can be seen in Fig. 10 as an indicator of the performance characteristics.

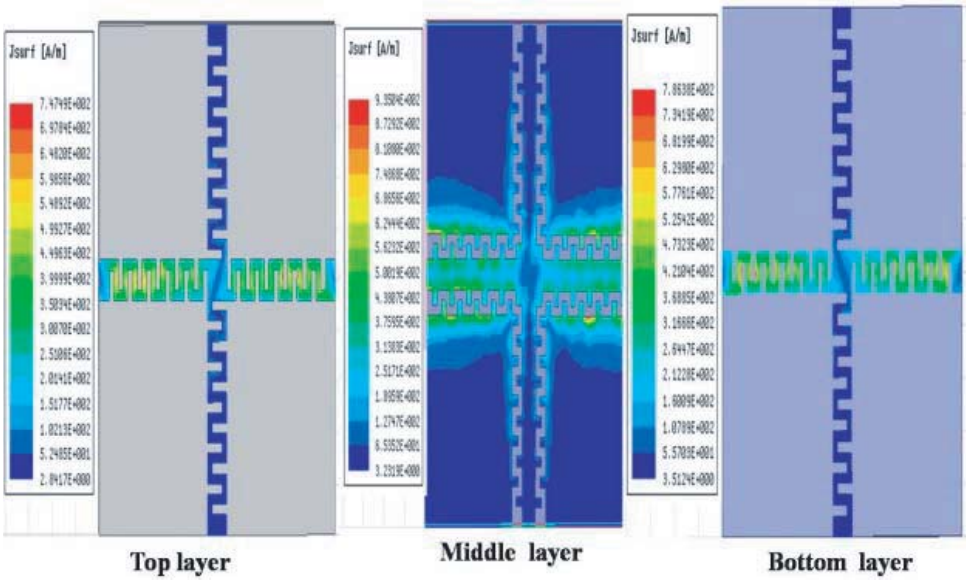

Figure 10. Surface current distribution at 10.5 GHz frequency.

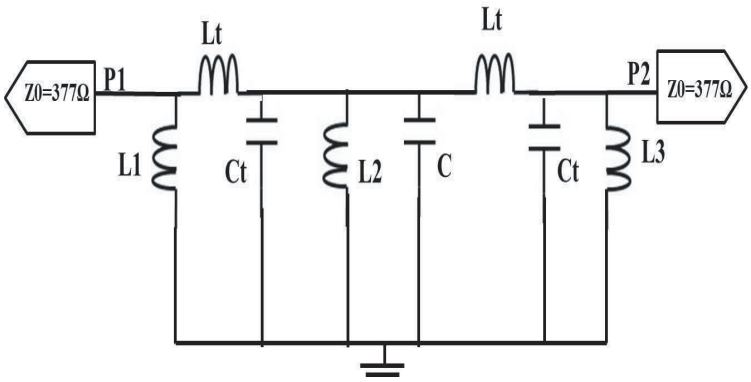

Figure 11. Equivalent circuit model of the proposed FSS.

4. EQUIVALENT CIRCUIT MODEL OF THE PROPOSED FSS

To verify the performance of the proposed structure, a simple equivalent circuit model is shown in Fig. 11. In this figure, the non-resonant middle layer was modeled with parallel inductors L2 and capacitor C since it is a square slot array layer, while the inductive resonant layers of the top and bottom layers were modeled as an inductor (L1) and the inductor (L3). All these layers were separated from each other with a Rogers RT/Duroid dielectric substrate layer, with the thickness of 0.25 mm which was modeled by two transmission line (Lt and Ct) equations calculated from the Telegraphs model for dielectric substrate (TEM transmission line) by using following Equations (1) and (2).

$$L_t = \mu_0 \mu_r T \tag{1}$$

$$C_t = \varepsilon_0 \varepsilon_r T \tag{2}$$

In the above equations 'T' is the substrate thickness, and μ_0 (free space permeability) $= 4\pi \times 10^{-7}$ H/m, whereas ε_0 (free space permittivity) $= 8.85 \times 10^{-12}$ F/m. Besides, after simplifying Eqs. (1) and (2) the parameters were obtained for dielectric substrate transmission line equation model as $L_t = 0.314$ nH and $C_t = 5.15$ fF.

The equations for calculating the inductance L1, L2, and L3, and capacitance C were obtained by

using the equations in [22].

$$L = \mu_0 \mu_{eff} \frac{P \cos\theta}{2\pi} \ln \frac{1}{\sin \frac{\pi w}{2P}} \tag{3}$$

$$C = 4\varepsilon_0 \varepsilon_{eff} \frac{P \cos\theta}{2\pi} \ln \frac{1}{\sin \frac{\pi g}{2P}} \tag{4}$$

After simplifying Marcuvitz Equations (3) and (4) for the given dimensions of the proposed FSS structure, the LC circuit parameters after being optimized using ADS (Advanced design system) software were obtained as $L1 = 8.07\,\text{nH}$, $L2 = 1.083\,\text{nH}$, $L3 = 2.8241\,\text{nH}$, and $C = 0.307\,\text{pF}$. To validate the proposed structures there is a comparison table which compares similar works (see Table 1). From Table 1 it is clearly seen that the proposed FSS has the smallest thickness.

Table 1. Comparison to other proposed FSS's.

FSS	Frequency (GHz)	Overall thickness	Element size	Order
13	10	0.033λ	0.15λ	2
14	21	0.273λ	0.21λ	2
15	3.8	0.038λ	0.076λ	2
16	8.5	0.257λ	0.2λ	3
18	10.6	0.056λ	0.215λ	2
This work	10.5	0.0177λ	0.175λ	1

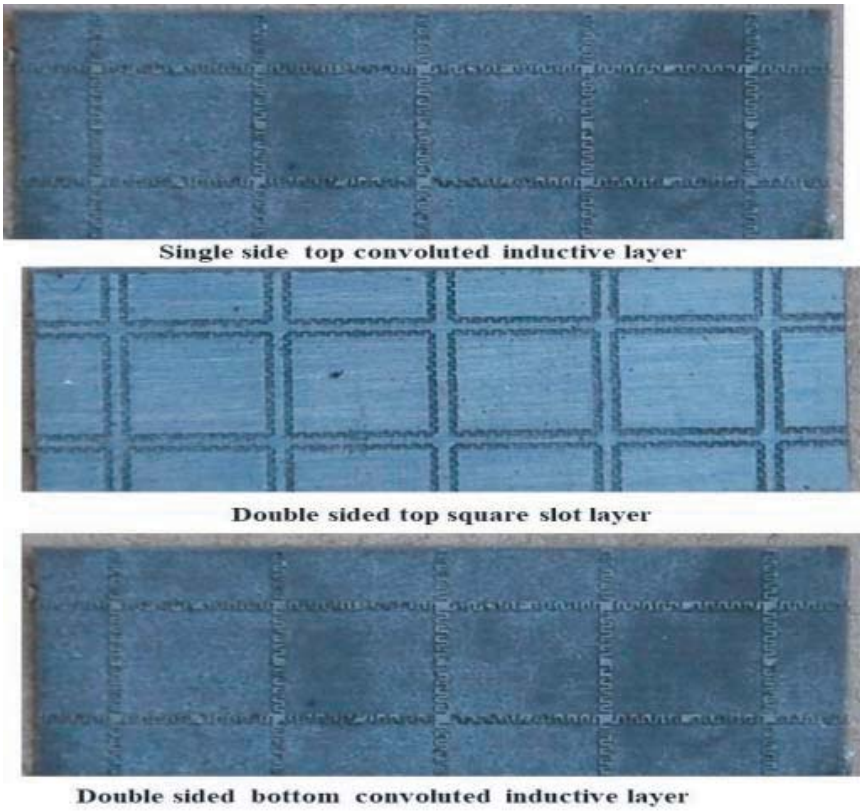

Figure 12. Fabricated FSS sheet.

5. MEASUREMENT PROCEDURE AND RESULTS

To establish the expediency of the unit cell design, a 10.2 mm × 25 mm FSS sheet of 2 × 5 cells was fabricated. Fig. 12 shows the single (for top layer) and double-sided layers (for middle and bottom layer) of the FSS sheet. Free space measurement of the Rogers substrate FSS sheet would increase the fabrication cost, so waveguide measurement, which was more economical, was performed instead. The experimental verification was performed with two WR 90 adapters and two WR 90 wave guide H plane bends, along with a vector network analyzer (VNA) with a waveguide measurement facility and a bandwidth range from 8.2 GHz to 12.4 GHz, as shown in Fig. 13. Before placing the proposed structure in the sample holder (made up of two WR 90 wave guide H plane bends), the waveguide calibration was performed. Waveguide calibration was performed using the short-short load thru (SSLT) calibration

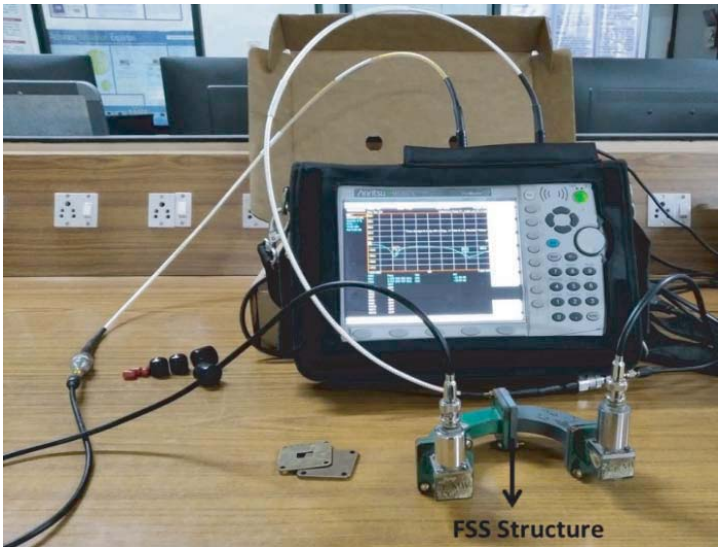

Figure 13. Measurement setup.

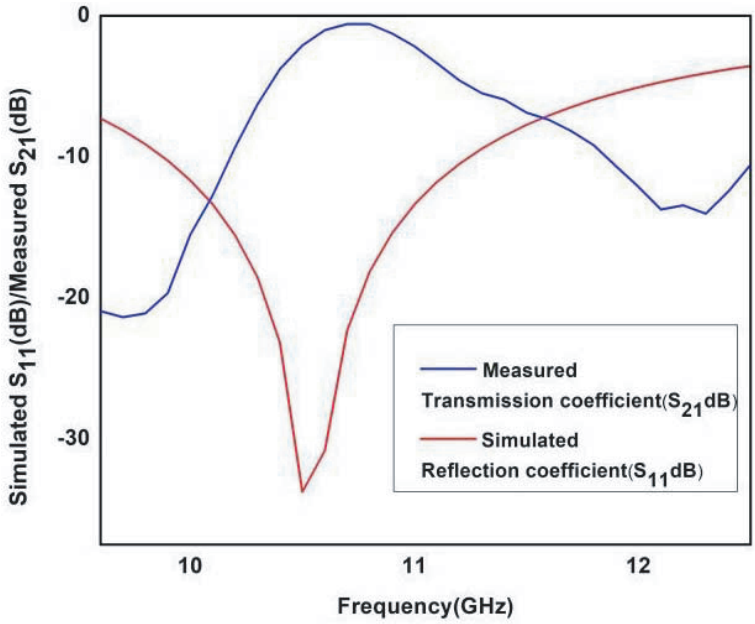

Figure 14. Comparison between measured and simulated results.

method. After successful calibration, the proposed sample was placed in between the sample holders to obtain the results. The proposed sample was placed in between the sample holders to obtain the results.

In this type of measurement, the measurement accuracy depends on the WR90 waveguide calibration, cable losses, and fabrication tolerances. The waveguide measurement was useful only in terms of finding the normal incidence angle only. However, it can be observed from Fig. 14 that the measured and simulated results were in good agreement. This method is quick to validate the simulated results, but the measurement inconsistency is more due to calibration errors and losses present in the setup. This is only a short study, and the full potential of the experiment needs conventional free space measurement in order to prove the stability and selective properties of frequency selective surfaces.

6. CONCLUSION

This paper presented a miniaturized low profile and ultra-thin frequency selective surface with a first-order band pass filtering response. The overall thickness of the proposed FSS structure was 0.0177λ for the prototype, which is very compact compared to the miniaturized structures proposed in earlier research. The proposed structure was also compared with a structure that was not convoluted, and finally the structure was fabricated and measured to verify the simulated results. Despite lacking free space environment testing, which is entirely a financial constraint, it was successfully tested in waveguide measurement. The proposed FSS structure was useful for ultra-thin band pass filtering prototype applications. The proposed FSS structure was insensitive to the angle of incidence and to the type of polarization. The proposed design method yielding these features has appeal in terms of applications that require ultra-thin profiles. However, further research is necessary to explore multi-band and wide-band applications.

REFERENCES

1. Wu, G., V. Hansen, H. P. Gemuend, and E. Kreysa, "Multi-layered submillimeter FSS of shifted crossed slot elements for applications in radio astronomy," *Proceedings of German Microwave Conference*, 2005.
2. Erkmen, F., T. S. Almoneef, and O. M. Ramahi, "Scalable electromagnetic energy harvesting using frequency-selective surfaces," *IEEE Transactions on Microwave Theory and Techniques*, Vol. 66, No. 5, 2433–2441, 2018.
3. Kiani, G. I., L. G. Olsson, A. Karlsson, and K. P. Esselle, "Transmission of infrared and visible wavelengths through energy-saving glass due to etching of frequency-selective surfaces," *IET Microwaves, Antennas & Propagation*, Vol. 4, No. 7, 955–961, 2010.
4. Sanchez-Escuderos, D., H. C. Moy-Li, E. Antonino-Daviu, M. Cabedo-Fabres, and M. Ferrando-Bataller, "Microwave planar lens antenna designed with a three-layer frequency-selective surface," *IEEE Antennas and Wireless Propagation Letters*, Vol. 16, 904-907, 2016.
5. Bouslama, M., M. Traii, T. A. Denidni, and A. Gharsallah, "Reconfigurable frequency selective surface for beam-switching applications," *IET Microwaves, Antennas & Propagation*, Vol. 11, No. 1, 69–74, 2017.
6. Lazaro, A., A. Ramos, D. Girbau, and R. Villarino, "A novel UWB RFID tag using active frequency selective surface," *IEEE Transactions on Antennas and Propagation*, Vol. 61, No. 3, 1155–1165, 2012.
7. Wu, P., F. Bai, Q. Xue, X. Liu, and S. R. Hui, "Use of frequency-selective surface for suppressing radio-frequency interference from wireless charging pads," *IEEE Transactions on Industrial Electronics*, Vol. 61, No. 8, 3969–3977, 2013.
8. Li, M. and N. Behdad, "Frequency selective surfaces for pulsed high-power microwave applications," *IEEE Transactions on Antennas and Propagation*, Vol. 61, No. 2, 677–687, 2012.
9. Li, L., J. Wang, J. Wang, H. Ma, H. Du, J. Zhang, and Z. Xu, "Reconfigurable all-dielectric meta material frequency selective surface based on high-permittivity ceramics," *Scientific Reports*, Vol. 6, 24178, 2012.

10. Sheng, X. J., J. J. Fan, N. Liu, and C. B. Zhang, "A miniaturized dual-band FSS with controllable frequency resonances," *IEEE Microwave and Wireless Components Letters*, Vol. 27, No. 10, 915–917, 2017.
11. Sheng, X., J. Fan, N. Liu, and C. Zhang, "A dual-band fractal FSS with SZ curve elements," *IEICE Electronics Express*, Vol. 14, No. 20170518, 2017.
12. Sarabandi, K. and N. Behdad, "A frequency selective surface with miniaturized elements," *IEEE Transactions on Antennas and Propagation*, Vol. 55, No. 5, 1239–1245, 2007.
13. Al-Joumayly, M. and N. Behdad, "A new technique for design of low-profile, second-order, bandpass frequency selective surfaces," *IEEE Transactions on Antennas and Propagation*, Vol. 57, No. 2, 452–459, 2009.
14. Abadi, S. M. A. M. H. and N. Behdad, "Inductively-coupled miniaturized-element frequency selective surfaces with narrowband, high-order bandpass responses," *IEEE Transactions on Antennas and Propagation*, Vol. 63, No. 11, 4766–4774, 2015.
15. Hussein, M., J. Zhou, Y. Huang, and B. Al-Juboori, "A low-profile miniaturized second-order bandpass frequency selective surface," *IEEE Antennas and Wireless Propagation Letters*, Vol. 16, 2791–2794, 2017.
16. Gao, M., S. M. A. M. H. Abadi, and N. Behdad, "A hybrid miniaturized-element frequency selective surface with a third-order bandpassresponse," *IEEE Antennas and Wireless Propagation Letters*, Vol. 16, 708–711, 2016.
17. Abadi, S. M. A. M. H. and N. Behdad, "Wideband linear-to-circular polarization converters based on miniaturized-element frequency selective surfaces," *IEEE Transactions on Antennas and Propagation*, Vol. 64, No. 2, 525–534, 2015.
18. Taghizadeh, M. and M. Maddahali, "New class of frequency selective surface based on non-resonant elements with high stability," *IET Microwaves, Antennas & Propagation*, Vol. 12, No. 3, 406–409, 2018.
19. Yin, W., H. Zhang, T. Zhong, and X. Min, "Ultra-miniaturized low-profile angularly-stable frequency selective surface design," *IEEE Transactions on Electromagnetic Compatibility*, Vol. 61, No. 4, 1234–1238, 2018.
20. Yu, Z., X. Yang, J. Zhu, C. Wang, Y. Shi, and W. Tang, "Dual-band three-dimensional FSS with high selectivity and small band ratio," *Electronics Letters*, Vol. 55, No. 14, 798–799, 2019.
21. Zhao, P. C., Z. Y. Zong, W. Wu, B. Li, and D. G. Fang, "Miniaturized-element bandpass FSS by loading capacitive structures," *IEEE Transactions on Antennas and Propagation*, Vol. 67, No. 5, 3539–3544, 2019.
22. Marcuvitz, N., *Waveguide Handbook*, Boston Technical Publishers, Lexington, MA, 1964.